# Craniovertebral Junction: Normal Anatomy, Craniometry, and Congenital Anomalies[1]

*Wendy R. K. Smoker, MD*

The craniovertebral junction (CVJ) comprises the occiput, atlas, and axis and is visible in most magnetic resonance (MR) imaging studies of the brain. Craniometric measurements used in radiologic assessment of CVJ anomalies include the Chamberlain line, Wackenheim clivus baseline, Welcher basal angle, and atlantooccipital joint axis angle. Most anomalies of the occiput are associated with decreased skull base height and basilar invagination, the latter being a primary developmental anomaly in which the vertebral column is abnormally high and prolapsed into the skull base. Occiput anomalies include condylus tertius, condylar hypoplasia, basiocciput hypoplasia, and atlantooccipital assimilation. Most atlas anomalies produce no abnormal CVJ relationships and are not associated with basilar invagination. These anomalies include aplasias, hypoplasias, and clefts of the atlas arches and "split atlas" (ie, posterior arch rachischisis associated with anterior arch rachischisis). Except for fusion anomalies, abnormalities of the axis are primarily confined to the odontoid process and are not associated with basilar invagination. These anomalies include persistent ossiculum terminale, odontoid aplasia, and os odontoideum. With the widespread availability of MR imaging, which is well suited for evaluating the CVJ because of its direct sagittal imaging capabilities, renewed understanding of CVJ anatomy and anomalies is important for all radiologists.

**Abbreviation:** CVJ = craniovertebral junction

**Index terms:** Skull, abnormalities, 127.147 • Skull, anatomy • Skull, MR, 127.12141 • Spine, abnormalities, 31.147 Spine, anatomy • Spine, MR, 31.12141

**RadioGraphics 1994;** 14:255–277

[1] From the Department of Radiology, Section of Neuroradiology, Medical College of Virginia, 1200 E Marshall St, MCV Station, Box 615, Richmond, VA 23298. Recipient of a Cum Laude award for a scientific exhibit at the 1992 RSNA scientific assembly. Received April 28, 1993; revision requested June 14 and received November 15; accepted November 15. **Address reprint requests to** the author.

## ■ INTRODUCTION

The craniovertebral (or craniocervical) junction (CVJ) is a collective term that refers to the occiput (posterior skull base), atlas, axis, and supporting ligaments. It encloses the soft-tissue structures of the cervicomedullary junction (medulla, spinal cord, and lower cranial nerves). Detailed discussions of the CVJ are conspicuously absent in many standard textbooks and chapters addressing the skull or cervical spine, since it lies "in between" these regions.

With the virtual extinction of polytomography in many institutions, detailed evaluation of this region fell to the realm of computed tomography (CT) or CT myelography. Unfortunately, adequate evaluation of the CVJ necessitates coronal and sagittal images, which, with CT, are available only as reconstructed images. This latter technique requires a large number of overlapping, thin-section axial images and an extremely cooperative patient. Now, with the widespread availability of magnetic resonance (MR) imaging, the CVJ is seen in virtually every sagittal MR imaging study of the brain. In essence, we are given a "free look" at the CVJ on a daily basis in a large number of patients undergoing MR imaging.

It, therefore, becomes important to become reacquainted with the signs and symptoms associated with CVJ pathologic conditions, the normal anatomy and basic craniometry used for assessing CVJ relationships, and the variety of congenital anomalies affecting this region. These topics are discussed herein, as well as the terminology applied to congenital abnormalities in the CVJ. Congenital anomalies are presented according to the structure primarily involved: the occiput, atlas, and axis.

Before reading this article, the reader is invited to assess his or her acumen in evaluating the CVJ by diagnosing the five anomalies presented on midsagittal MR images as unknowns in Figure 1. All of these cases are reviewed in subsequent discussions, and the diagnoses are presented after the summary section.

## ■ SIGNS AND SYMPTOMS OF CVJ ABNORMALITIES

The signs and symptoms of CVJ abnormalities are varied, typically begin insidiously and arise fairly late, progress slowly, remain stationary, and rarely relapse (1). They may be referable to the cervical spinal cord, the brain stem, cerebellum, cervical nerve roots, lower cranial nerves, or the vascular supply to these structures (Table) (2). Although the majority of signs and symptoms may lead the patient to a neurologist or neurosurgeon, a number of them that signify cranial nerve deficits (eg, vertigo, dysphagia, facial paralysis, decreased hearing, tongue atrophy) may prompt referral to an otolaryngologist. It is, therefore, important to become familiar with the varied manifestations of CVJ pathologic conditions so that appropriate imaging studies are performed when these patients present for evaluation.

In some patients with one of the more common congenital anomalies of this region (eg, atlantooccipital assimilation), a fairly characteristic clinical picture may be present: short broad neck, elevation of the scapula, low hairline, and limitation of neck movement (2). The anomaly may also be associated with abnormalities of the jaw, incomplete clefting of nasal cartilages, cleft palate, ear deformities, cervical ribs, hypospadias, and urinary tract anomalies (2).

**Signs and Symptoms of CVJ Abnormalities**

- Motor myelopathy
  - May be quite subtle and nonspecific
  - May be manifest only by lack of endurance
  - May be quadriparesis, triparesis, paraparesis, hemiparesis, or monoparesis
- Sensory abnormalities
  - Posterior column dysfunction
  - Hypalgesia (spinothalamic tract dysfunction)
  - Bladder dysfunction (urgency or hesitation)
- Brain stem dysfunction
  - Nystagmus (horizontal or downbeat)
  - Apnea
  - Ataxia
  - Dysmetria
  - Internuclear ophthalmoplegia
  - Facial diplegia
- Lower cranial nerve dysfunction
  - Decreased hearing
  - Dysphagia
  - Soft palate paralysis
  - Trapezius muscle weakness
  - Tongue atrophy
- Vascular compromise
  - Syncope
  - Vertigo
  - Intermittent paresis

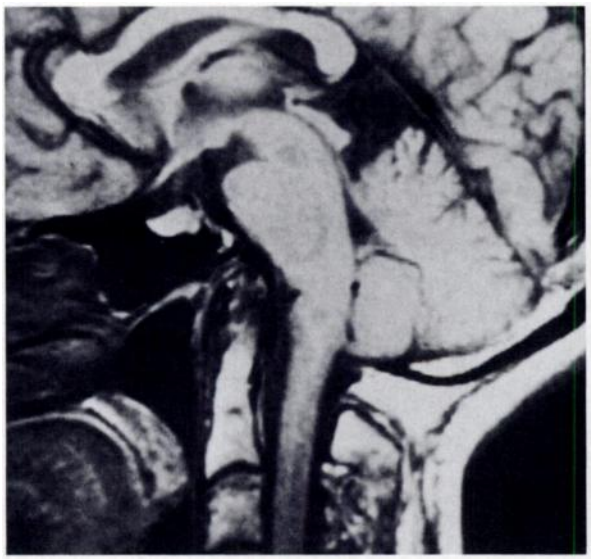

a.

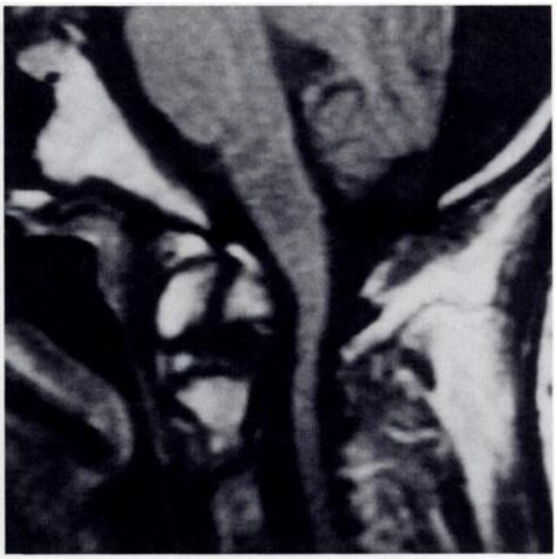

b.

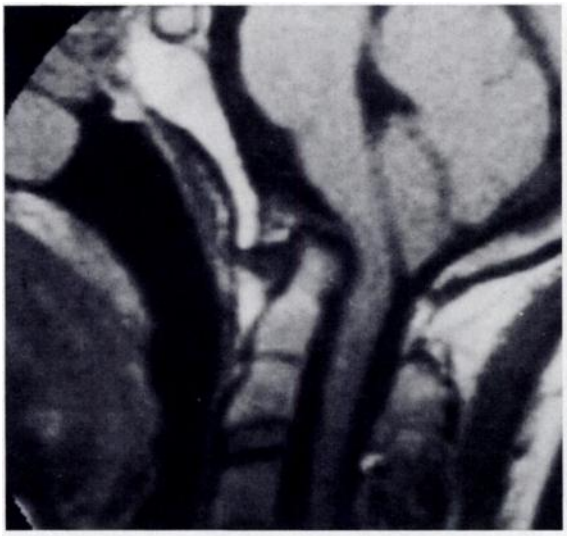

c.

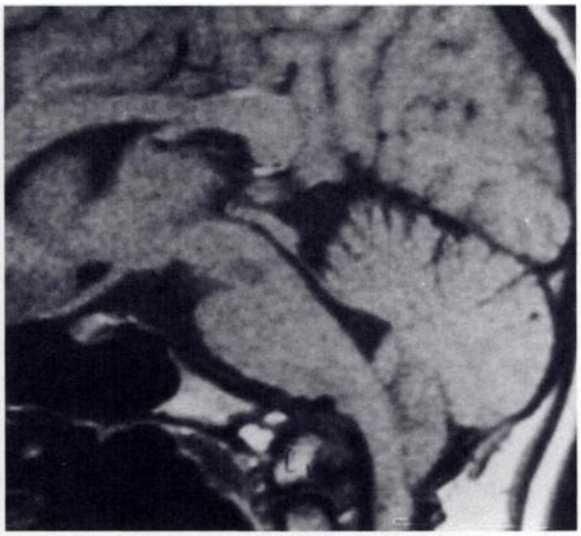

d.

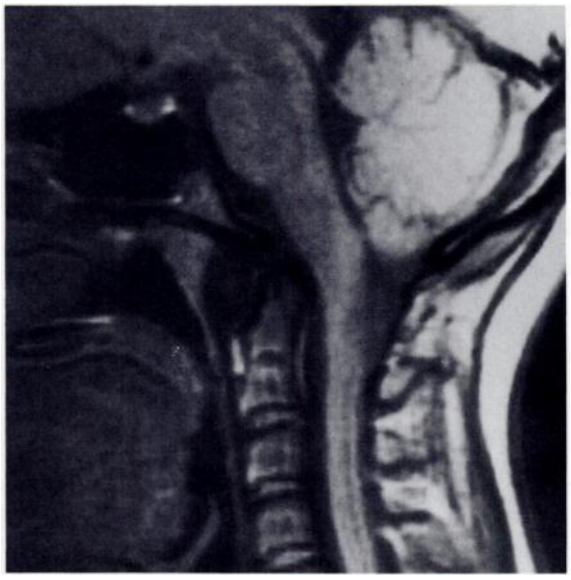

e.

**Figure 1.** Unknown cases. Each of the five images **(a–e)** illustrates a congenital anomaly of the CVJ. Test your current knowledge of this region by diagnosing each anomaly (the diagnoses are presented after the summary section).

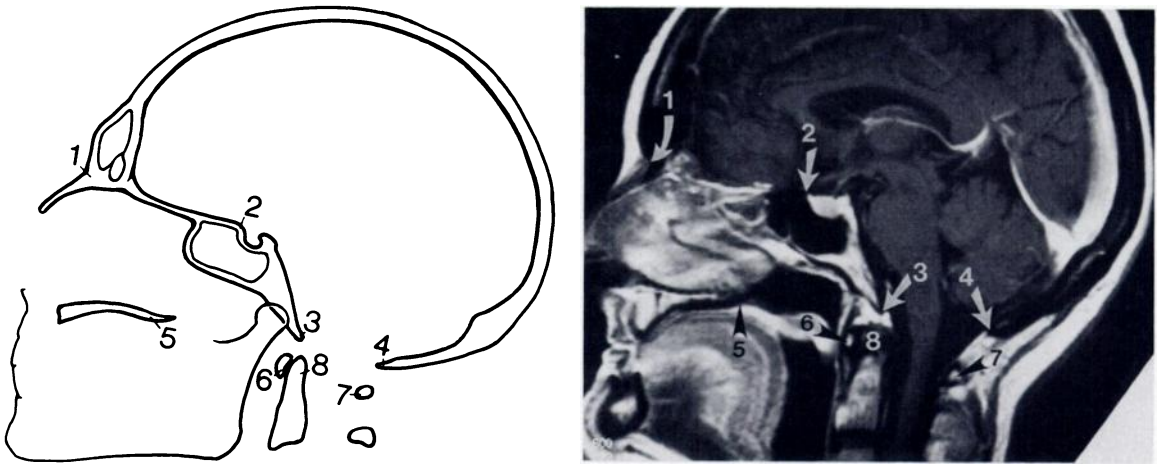


a. b.

**Figure 2.** Normal landmarks on lateral views needed to assess CVJ relationships and perform basic craniometric measurements. Diagram **(a)** and midsagittal T1-weighted (repetition time in msec/echo time in msec [700/20]) MR image **(b)** demonstrate the nasion (*1*), tuberculum sella (*2*), basion (anterior margin of the foramen magnum) (*3*), opisthion (posterior margin of the foramen magnum) (*4*), posterior pole of the hard palate (*5*), anterior arch of the atlas (*6*), posterior arch of the atlas (*7*), and odontoid process (*8*).

## ■ BASIC CVJ CRANIOMETRY

Radiologic evaluation of the CVJ requires identification of only a few anatomic structures, knowledge of some basic osseous relationships, and a few craniometric measurements (Figs 2, 3). Some of these anatomic landmarks (eg, nasion, tuberculum, hard palate) require views of the skull and not views of the cervical spine.

Over the years, multiple lines, planes, and angles have been described for assessment of CVJ relationships, initially with radiography and later with polytomography. There is a certain disadvantage in all of these measurements because the anatomic structures and planes vary within a normal range (1). In all cases, more than one measurement should be assessed. Two lines have remained particularly useful for evaluation of CVJ relationships with virtually any imaging modality: the Chamberlain line and the Wackenheim clivus baseline. Although used less frequently, two angles also continue to be useful: the Welcher basal angle and the atlantooccipital joint axis angle.

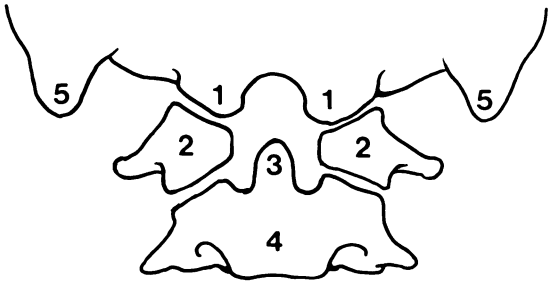


a.

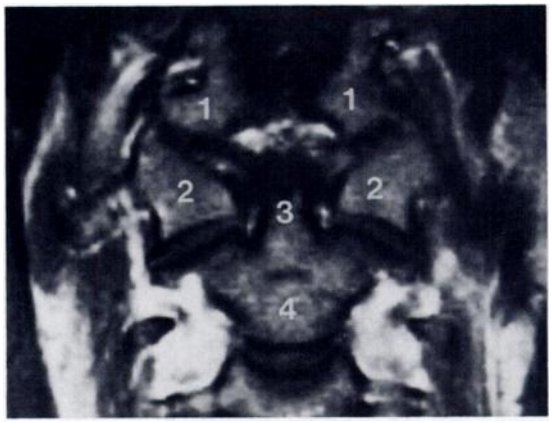


b.

**Figure 3.** Normal landmarks on coronal views needed to assess CVJ relationships and perform basic craniometric measurements. Diagram **(a)** and coronal T1-weighted (700/20) MR image **(b)** demonstrate the occipital condyles (*1*), lateral masses of the atlas (*2*), odontoid process (*3*), axis body (*4*), and tips of the mastoid processes (*5*) (the last is seen only in the diagram).

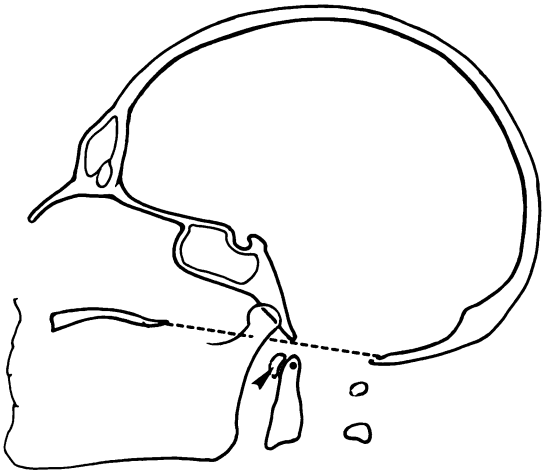

a.

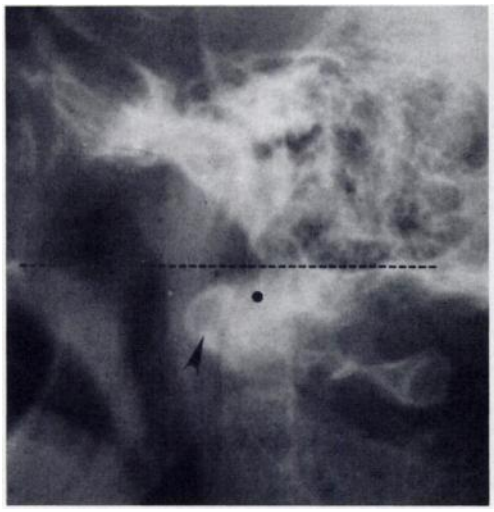

b.

c.

**Figure 4.** Chamberlain line. Diagram **(a)**, lateral radiograph **(b)**, and midsagittal T1-weighted (600/20) MR image **(c)** demonstrate the Chamberlain line (dashed and solid line) drawn between the posterior pole of the hard palate and the opisthion. The anterior arch of the atlas (arrowhead) and the odontoid process (dot) lie below this line.

## • Chamberlain Line

The Chamberlain line extends between the posterior pole of the hard palate and the opisthion (posterior margin of the foramen magnum) (Fig 4) (3). McGregor (4) developed a modification of the Chamberlain line when the opisthion could not be identified on plain radiographs. This McGregor line extends between the posterior pole of the hard palate and the lowest point of the occipital squamosal surface. The tip of the odontoid process commonly lies below or just tangent to the Chamberlain line, and it may normally project above this line for a distance of several millimeters. The maximum distance that the odontoid process may be seen above this line is variably reported in the literature, ranging from 1 mm ± 3.6 to 6.6 mm (1–5). The odontoid tip may be slightly higher if the McGregor line is used. The anterior arch of the atlas typically lies below these lines.

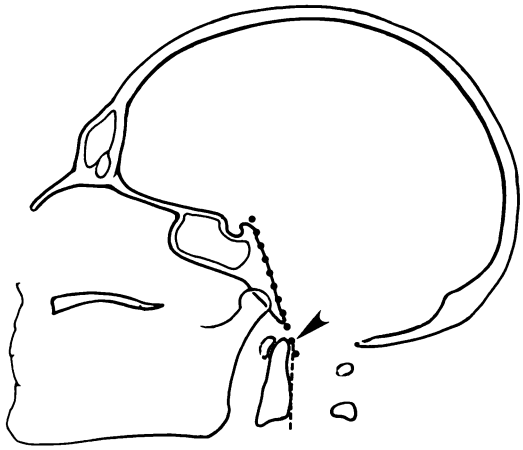

5a.

6a.

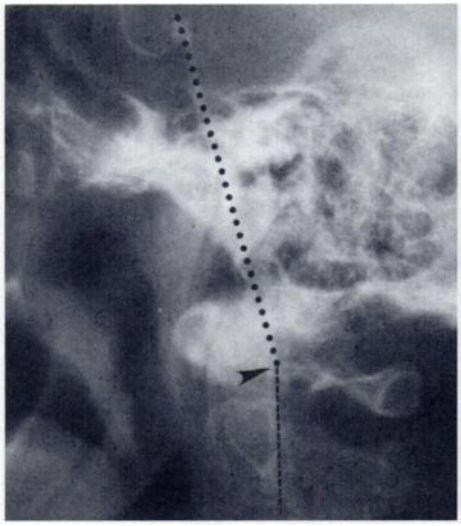

5b.

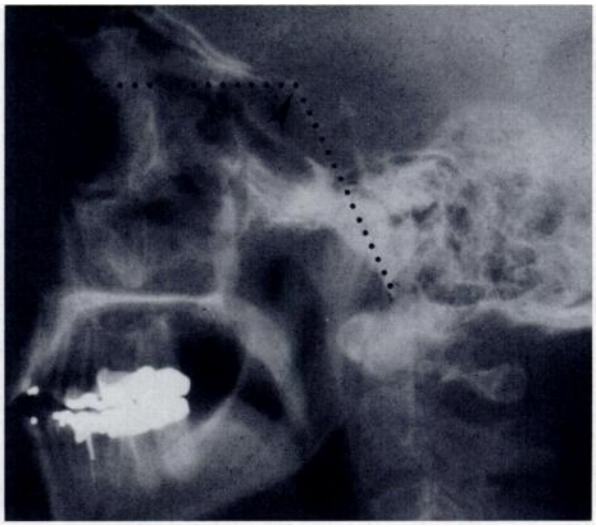

6b.

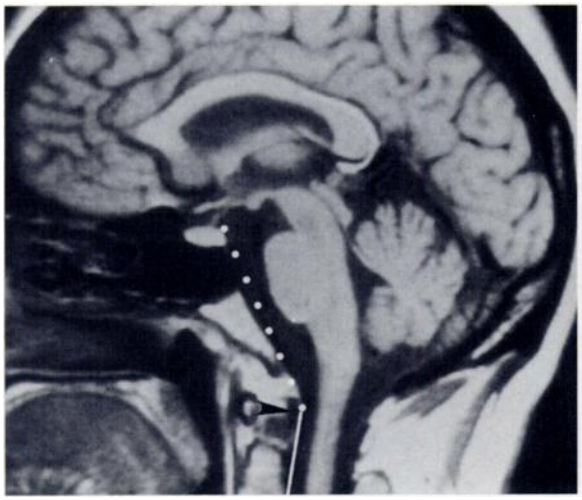

5c.

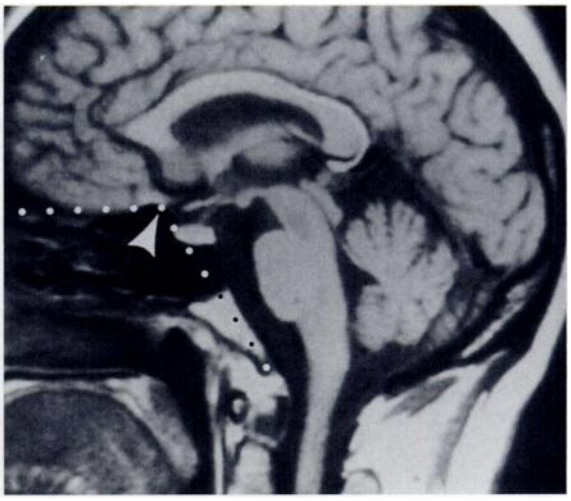

6c.

**Figures 5, 6.** **(5)** Wackenheim clivus baseline. Diagram **(a)**, lateral radiograph **(b)**, and midsagittal T1-weighted (600/20) MR image **(c)** demonstrate the Wackenheim line (dotted line), which is drawn along the clivus and extrapolated inferiorly (dashed and solid lines). The line falls tangent to the posterior aspect of the odontoid process. The clivus-canal angle (arrowhead) should range between 150° and 180°. **(6)** Welcher basal angle. Diagram **(a)**, lateral radiograph **(b)**, and midsagittal T1-weighted (600/20) MR image **(c)** demonstrate the Welcher angle (arrowhead) formed between the nasion-tuberculum and tuberculum-basion lines (dotted lines). The angle should be 140° or less.

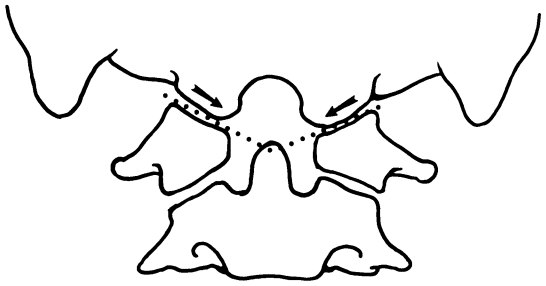

a.

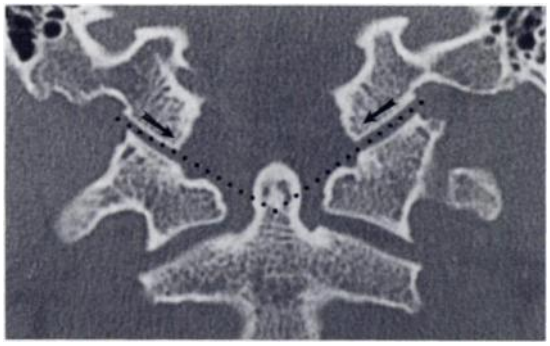

b.

c.

**Figure 7.** Atlantooccipital joint axis angle. Diagram **(a)**, coronal CT scan **(b)**, and coronal T1-weighted (600/20) MR image **(c)** demonstrate the atlantooccipital joint axis angle formed at the intersection of lines drawn through the atlantooccipital joints (dotted lines). The angle should range between 124° and 127°. If the mastoid tips were connected (bimastoid line), the entirety of the odontoid process would lie below this line. The skull base should descend as it approaches midline (arrows).

### • Wackenheim Clivus Baseline

The Wackenheim clivus baseline (also referred to as the basilar line) is constructed by drawing a line along the clivus and extrapolating it inferiorly into the upper cervical spinal canal (Fig 5). This line should fall tangent to the posterior aspect of the tip of the odontoid process (6). The angle formed at the intersection of the Wackenheim clivus baseline with a line constructed along the posterior surface of the axis body and odontoid process (craniovertebral or clivus-canal angle) normally ranges from 150° in flexion to 180° in extension (Fig 5) (2). Ventral spinal cord compression may occur when the angle is less than 150° (2).

### • Welcher Basal Angle

The Welcher basal angle is formed at the intersection of the nasion-tuberculum line and the tuberculum-basion line (Fig 6). It averages 132° and should always be less than 140° (1,7). This angle is increased when the skull base is abnormally flattened.

### • Atlantooccipital Joint Axis Angle

The atlantooccipital joint axis angle is formed by lines drawn parallel to the atlantooccipital joints, which typically intersect at the center of the odontoid process when the condyles are symmetric (Fig 7) (2). The average angle is 125°, with a range between 124° and 127° (1). This angle becomes more obtuse in the presence of occipital condyle hypoplasia.

## ■ TERMINOLOGY

The literature describing the CVJ continues to fuel the confusion related to this region, with the frequent, erroneous, interchangeable use of the terms "basilar invagination," "basilar impression," and "platybasia." These terms are not synonymous.

The term "basilar invagination" refers to a primary developmental anomaly in which the vertebral column is abnormally high and prolapsed into the skull base (2). Because the anomaly may be due to a number of causes (basiocciput hypoplasia, occipital condyle hypoplasia, various atlantooccipital assimilations), it might be best to think of basilar invagination as a radiographic finding and not a diagnosis in and of itself. If at all possible, one should attempt to define the underlying abnormality responsible for the basilar invagination. There is an increased prevalence of neural dysgenesis associated with basilar invagination, such as the Chiari malformation or syringohydromyelia, reported to occur in 25%–35% of these patients (2).

The term "basilar impression" should be reserved for the secondary or acquired form of basilar invagination. It results from softening of the skull base and is uncommon, mainly seen in association with Paget disease and osteomalacia (1). Other conditions that have been described in association with basilar impression include hyperparathyroidism, osteogenesis imperfecta, Hurler syndrome, rickets, and skull base infection (2). The term "cranial settling" is typically applied to the CVJ changes associated with rheumatoid arthritis (8).

Platybasia is an anthropometric term that refers to flattening of the skull base, manifested by an increase in the Welcher basal angle. Platybasia may occasionally be an isolated finding without associated basilar invagination (2). More often, however, basilar invagination is present.

Although the Chamberlain line and Wackenheim clivus baseline may not be violated, the craniovertebral or clivus-canal angle becomes abnormally acute (Fig 8). Normally 150° or greater, this angle may approach 90°

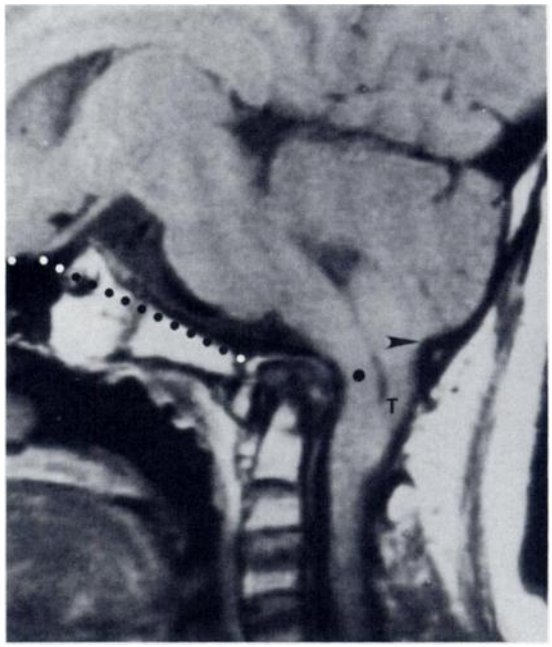


**Figure 8.** Platybasia. Midsagittal T1-weighted (600/20) MR image reveals marked platybasia. The Welcher basal angle (dotted line) measures 155°. The Chamberlain line and Wackenheim clivus baseline are not violated, but the clivus-canal angle measures 110°, producing marked bow-string deformity and compression of the cervicomedullary junction (dot). The cerebellar tonsils (*T*) extend far below the opisthion (arrowhead).

in some patients, producing bow-string deformity and marked compression of the cervicomedullary junction. It is best assessed on midsagittal MR images or lateral views of the skull.

## ■ THE OCCIPUT

The occipital bone is composed of basioccipital, exoccipital, and supraoccipital portions enclosing the foramen magnum (Fig 9a). The basiocciput, embryologically derived from fusion of four occipital sclerotomes (also referred to as primary cranial vertebrae), forms the lower portion of the clivus (Fig 9b) (2,9). The upper portion of the clivus is formed by the basisphenoid, separated from the basiocciput by the sphenooccipital synchondrosis. The age at which this synchondrosis fuses, as reported in the literature, ranges from "after the twelvth year" (1) to 14–16 years for girls

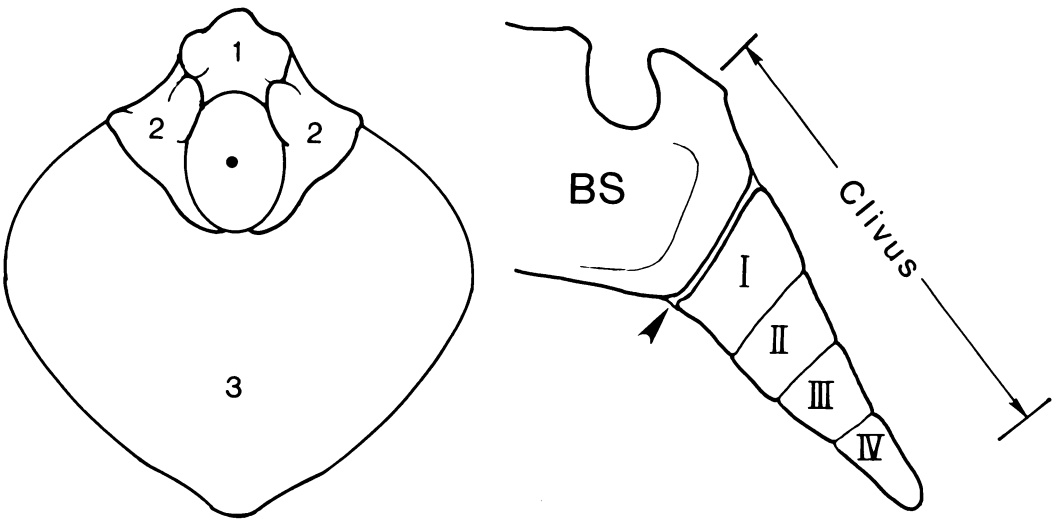


a. b.

**Figure 9.** Occipital bone. **(a)** Diagram illustrates the components of the occipital bone: basioccipital portion (*1*), exoccipital portion (*2*), and supraoccipital portion (*3*). The foramen magnum lies in the center (dot). **(b)** Diagram illustrates the contribution of the basiocciput, formed by four occipital sclerotomes, to the lower portion of the clivus. The upper portion is formed by the basisphenoid (*BS*). The sphenooccipital synchondrosis (arrowhead) lies in between.

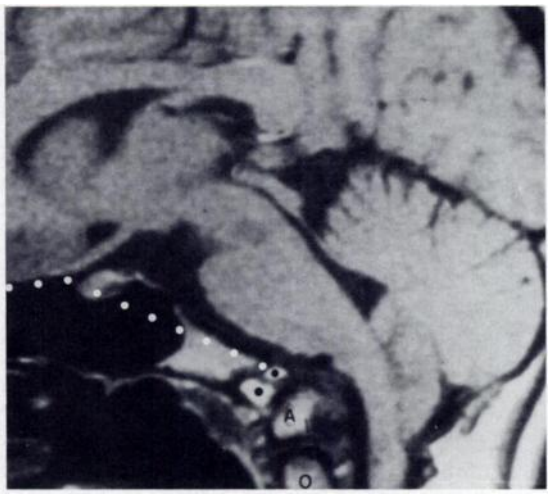


**Figure 10.** Condylus tertius and platybasia. Midsagittal T1-weighted (600/20) MR image reveals marked skull base flattening, with a Welcher basal angle of 150° (dotted line). Note the marked bowstring deformity of the cervicomedullary junction. The C-1 arch (*A*) lies directly above the tip of the odontoid process (*O*). Marrow within accessory ossification centers (condylus tertius) (black dots) is seen at the tip of the basion.

and 16–18.5 years for boys (2,9). Most occipital anomalies are associated with decreased skull base height and basilar invagination.

## • Condylus Tertius

Anomalies and malformations of the most caudal of the occipital sclerotomes are collectively termed "manifestations of occipital vertebrae" (2). When the hypochordal bow of the fourth occipital sclerotome (proatlas) persists or when the proatlas fails to integrate, an ossified remnant may be present at the distal end of the clivus, called the condylus tertius or third occipital condyle (1,2,5). Although typically single, multiple supranumerary ossicles may be present (Fig 10) (9). This third condyle may form a joint or pseudojoint with the odontoid process or with the anterior arch of the atlas and may lead to limitation in the range of motion of the CVJ (1). There is an increased prevalence of os odontoideum associated with this abnormality (2).

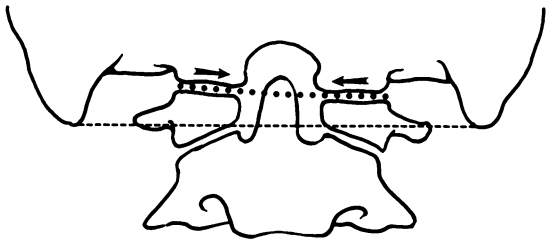

a.

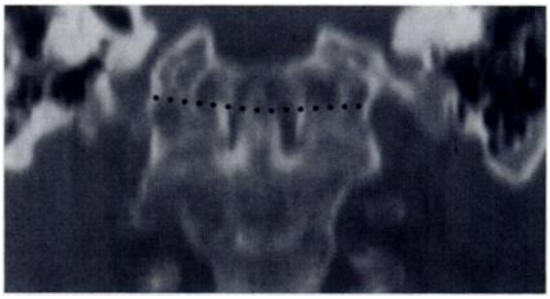

b.

**Figure 11.** Condylar hypoplasia. **(a)** Diagram illustrates marked widening of the angle formed by lines traversing the atlantooccipital joints (dotted line). Flattening of the skull base is evident (arrows). Note how far cephalad the tip of the odontoid process lies above a line drawn between the tips of the mastoid processes (dashed line). **(b)** Coronal CT scan reveals widening of the atlantooccipital joint axis angle (dotted line). The joints are extrapolated in this case, as the lateral C-1 masses are fused to the hypoplastic occipital condyles and seem to abut the jugular tubercles.

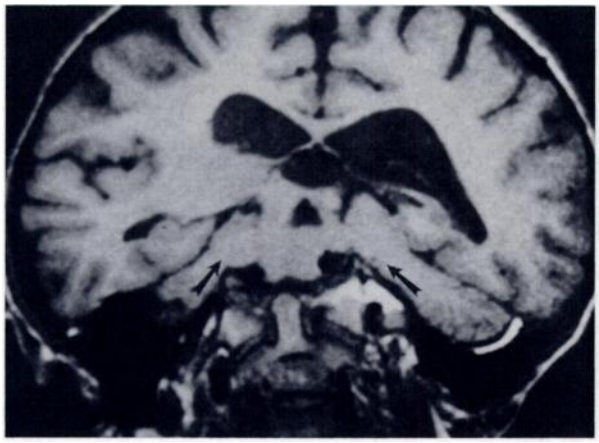

a.

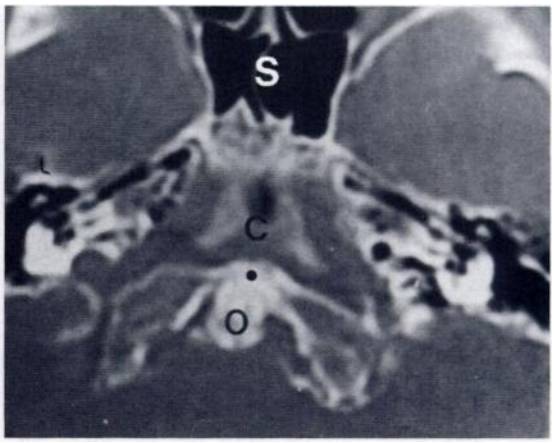


b.

**Figure 12.** Condylar hypoplasia. **(a)** Coronal T1-weighted (600/20) MR image shows the extreme upward slope to the skull base in the medial direction (arrows). **(b)** Axial CT scan obtained at the level of the ossicles demonstrates the sphenoid sinus (*S*), clivus (*C*), anterior arch of the atlas (dot), and odontoid process (*O*). It is markedly abnormal that all of these structures are visible on the same section.

## • Condylar Hypoplasia

In condylar hypoplasia, the occipital condyles are underdeveloped and have a flattened appearance, leading to basilar invagination (violation of the Chamberlain line) and widening of the atlantooccipital joint axis angle (Fig 11a). As seen in Figure 7, the skull base normally descends medially. In the presence of condylar hypoplasia, the skull base is flattened or even ascends medially (Figs 11, 12) (1). Whereas the tip of the odontoid process and the lateral masses of the atlas typically lie below a line connecting the mastoid tips (bimastoid line), this relationship is violated in condylar hypoplasia. The lateral masses of the atlas may be fused to the hypoplastic condyles, further accentuating the basilar invagination. Clinically, condylar hypoplasia limits, or may even abolish, movements at the atlantooccipital joint and may occasionally lead to compression of the vertebral artery secondary to excessive posterior gliding of the occiput in relation to the atlas (10).

## • Basiocciput Hypoplasia

Hypoplasia of the basiocciput may be mild or severe, depending on the number of occipital vertebrae affected. It results in shortening of the clivus and violation of the Chamberlain

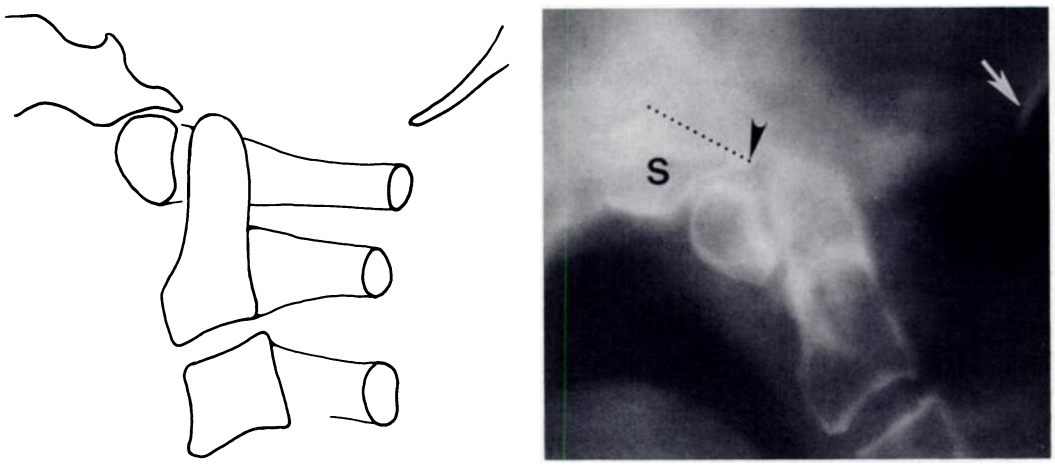


a. b.

**Figure 13.** Basiocciput hypoplasia. Diagram **(a)** and midline sagittal polytomogram **(b)** illustrate basilar invagination and violation of the Chamberlain line and Wackenheim clivus baseline. The entirety of the clivus (dotted line) is composed of the basisphenoid (*S*). The basiocciput is absent. The odontoid process lies at the plane of the foramen magnum, between the basion (arrowhead) and opisthion (arrow).

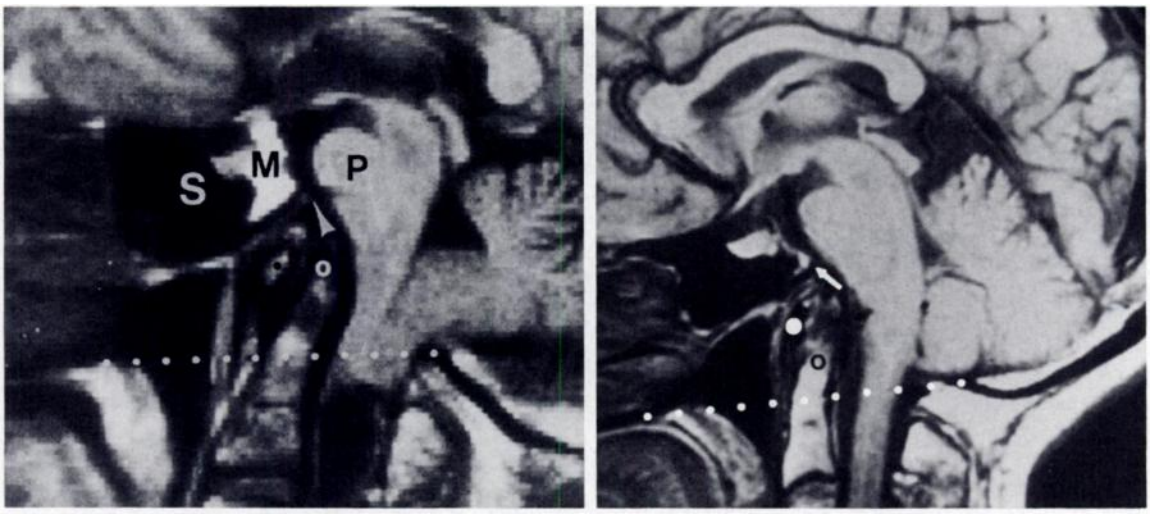


14. 15.

**Figures 14, 15.** Basiocciput hypoplasia. **(14)** Midsagittal T1-weighted (600/20) MR image reveals complete basiocciput hypoplasia with severe basilar invagination. The tip of the odontoid process (*o*) lies far above the Chamberlain line (dotted line), and the basion (arrowhead) lies at the middle of the pons (*P*). *S* = sphenoid sinus, *M* = marrow in the basisphenoid forming the entirety of the clivus, dot = anterior arch of the atlas. **(15)** Midsagittal T1-weighted (600/20) MR image demonstrates severe basiocciput hypoplasia and aplasia with the basion (arrow) at the middle of the pons. The tip of the odontoid process (*o*) and the anterior arch of the atlas (dot) are far above the Chamberlain line (dotted line), compatible with basilar invagination.

line and is virtually always associated with basilar invagination (Fig 13) (1,9). The Wackenheim clivus baseline is usually normal, although the clivus-canal angle is typically decreased and there may be bow-string deformity of the cervicomedullary junction. It is frequently impossible to identify the tip of the elevated odontoid process on lateral radiographs, although the presence of basilar invagination is usually obvious. These abnormal relationships, as well as the causative basiocciput hypoplasia, are all easily appreciated on midsagittal MR images (Figs 14, 15).

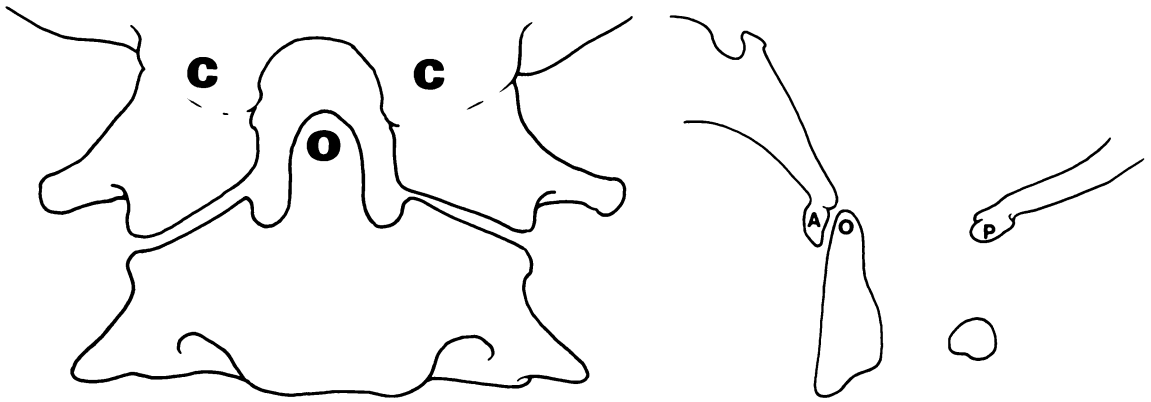


16a. 16b.

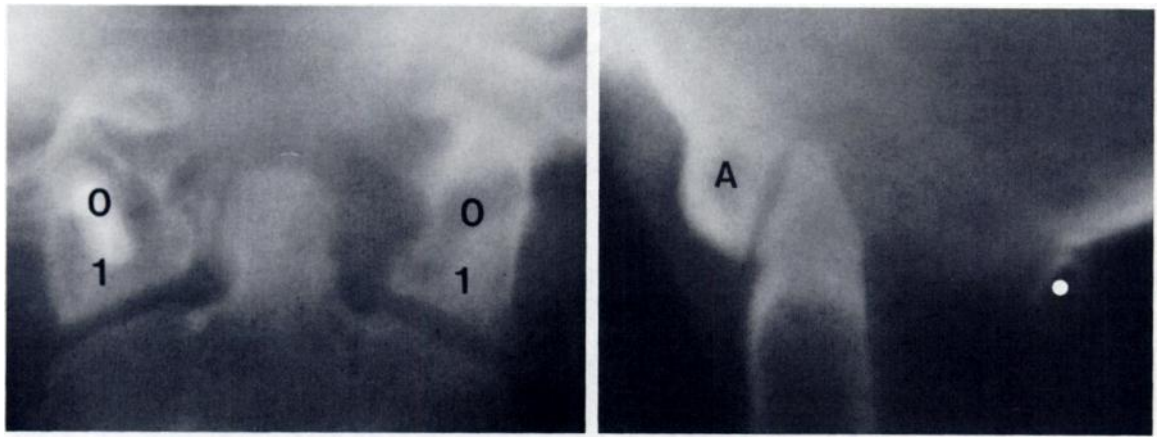


17a. 17b.

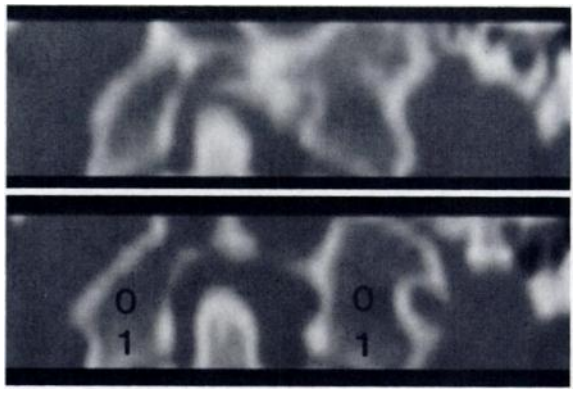


17c.

**Figures 16, 17.** **(16)** Complete atlantooccipital assimilation. Coronal **(a)** and midsagittal **(b)** diagrams illustrate the occipital condyles (*C*), odontoid process (*O*), anterior atlas arch (*A*), and posterior atlas arch (*P*). **(17)** Atlantooccipital assimilation. **(a)** Coronal polytomogram demonstrates complete fusion of the lateral C-1 masses (*1*) to the occipital condyles (*O*). **(b)** Midsagittal polytomogram reveals complete assimilation of the anterior arch (*A*) to the basion and probably the cortices of the posterior arch (dot) and the opisthion. **(c)** Coronal CT scans reveal complete assimilation of the lateral C-1 masses (*1*) and the occipital condyles (*O*). Eccentric positioning of the odontoid process at the C-1 level is demonstrated.

## • Atlantooccipital Assimilation

The failure of segmentation between the skull and first cervical vertebra results in assimilation of the atlas. The assimilation may be complete (Figs 16, 17) or partial. It invariably results in basilar invagination. Although the Wackenheim clivus baseline may be normal, the clivus-canal angle may be decreased. When incompletely assimilated, the atlas arches appear too high on the lateral plain radiograph or, when completely assimilated, are not visible at all (Fig 18). There is an increased prevalence of associated fusion of the axis and third cervical vertebra in association with atlantooccipital assimilation (11). When this is present, gradual loosening of the atlantodental joint with progressive atlantoaxial subluxation may occur, reported in approximately 50% of cases (Fig 19) (1,2). In some instances, atlantooccipital assimilation may be associated with sudden death (12).

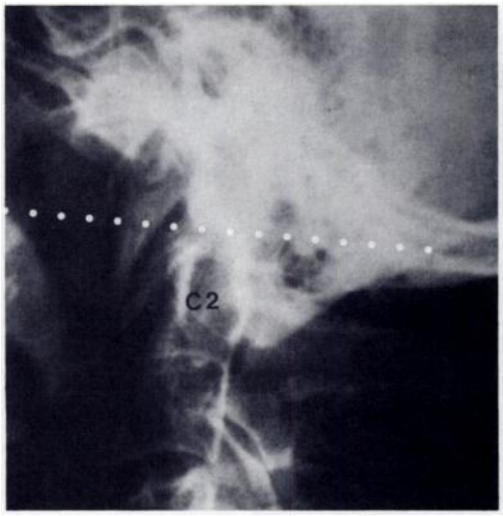


a.

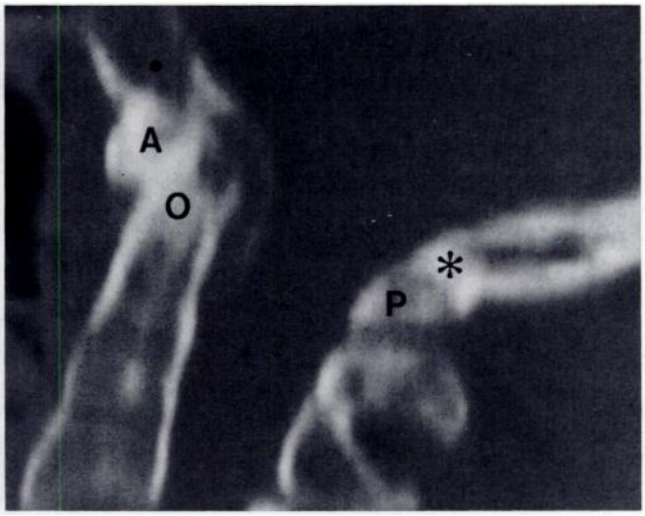


b.

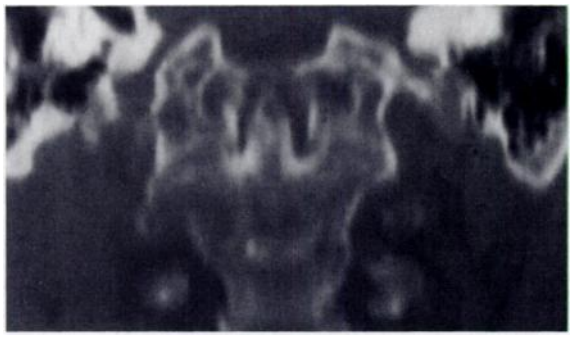

c.


d.

**Figure 18.** Atlantooccipital assimilation. **(a)** On the lateral radiograph, the atlas arches and odontoid process are not clearly identified. Basilar invagination, however, is suggested by the location of the Chamberlain line (dotted line) in relation to the remainder of the axis (*C2*). **(b)** Reconstructed midsagittal CT scan reveals assimilation of the anterior atlas arch (*A*) to the basion (dot) and the posterior arch (*P*) to the opisthion (*). The tip of the odontoid (*O*) lies well above the Chamberlain line (extrapolated) and may also be fused with the anterior atlas arch. **(c)** Reconstructed coronal CT scan reveals complete fusion of the hypoplastic occipital condyles to the lateral C-1 masses. Note the upward medial slope to the skull base. **(d)** Midsagittal T1-weighted (600/20) MR image also reveals the anterior arch (single dot) fused to the basion (arrow) and the posterior arch (double dots) fused to the opisthion (*). The Chamberlain line (dashed line) is violated.

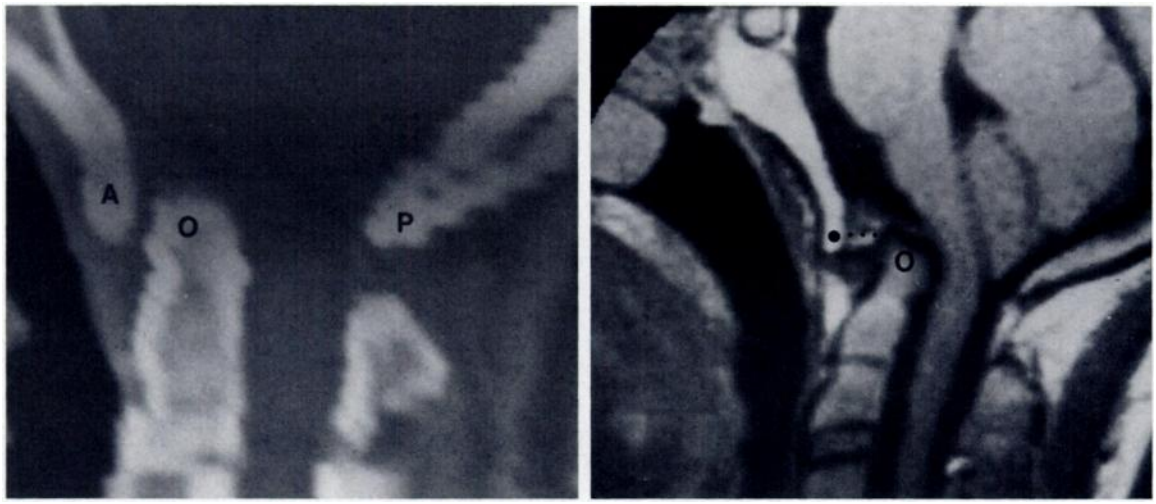


a. b.

**Figure 19.** Atlantooccipital assimilation with atlantoaxial subluxation. **(a)** Reconstructed midsagittal CT scan reveals complete atlas arch assimilation. The odontoid process (*O*) lies at the level of the foramen magnum. *A* = anterior arch, *P* = posterior arch. **(b)** Midsagittal T1-weighted (600/20) MR image reveals elongation and a "comma" configuration to the anterior lip of the foramen magnum produced by incorporation of the anterior atlas arch to the basion (dot). A similar finding is present at the posterior margin of the foramen magnum. There is a marked increase in the anterior atlantodental interval (dotted line) such that the displaced odontoid process (*O*) is markedly compressing the cervicomedullary junction. Also note incomplete segmentation of C-2 and C-3.

## ■ THE ATLAS

With the exception of the various atlantooccipital assimilations previously discussed, most atlas anomalies, when isolated, produce no abnormal CVJ relationships and are not associated with basilar invagination. The vast majority of anomalies consist of various arch clefts, aplasias, and hypoplasias, which can best be understood by knowledge of atlas ossification centers (Fig 20). Although they typically produce no abnormalities of CVJ relationships, arch anomalies are, not infrequently, mistaken for fractures in the evaluation of plain radiographs of patients with a history of cervical spine trauma. For this reason, it is important to be familiar with the gamut of arch anomalies.

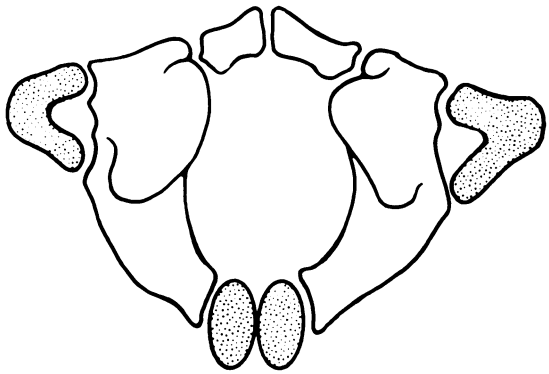

**Figure 20.** Atlas ossification centers. Diagram depicts the ossification centers of the atlas. Secondary centers are stippled.

### • Posterior Arch Anomalies

Total or partial aplasia of the posterior atlas arch is rare (13,14). Various types of developmental deficiencies have been described, including total aplasia, Keller-type aplasia with persistence of the posterior tubercle, aplasia with a unilateral or bilateral remnant and midline rachischisis, and hemiaplasia or partial hemiaplasia of the posterior arch (Fig 21) (1,13). Although absence of the posterior arch, when isolated, has been stated to be asymptomatic (15), reports of associated anterior atlantoaxial subluxation have been made (14), and bilateral atlantoaxial offset has been reported in association with both total and partial aplasias, simulating the Jefferson fracture (13).

In contrast to the aplasias and hypoplasias, clefts of the atlas arches are much more commonly observed. Posterior rachischisis, the most common, is observed in 4% of adult autopsy specimens (13). The vast majority of posterior atlas clefts (97%) are midline,

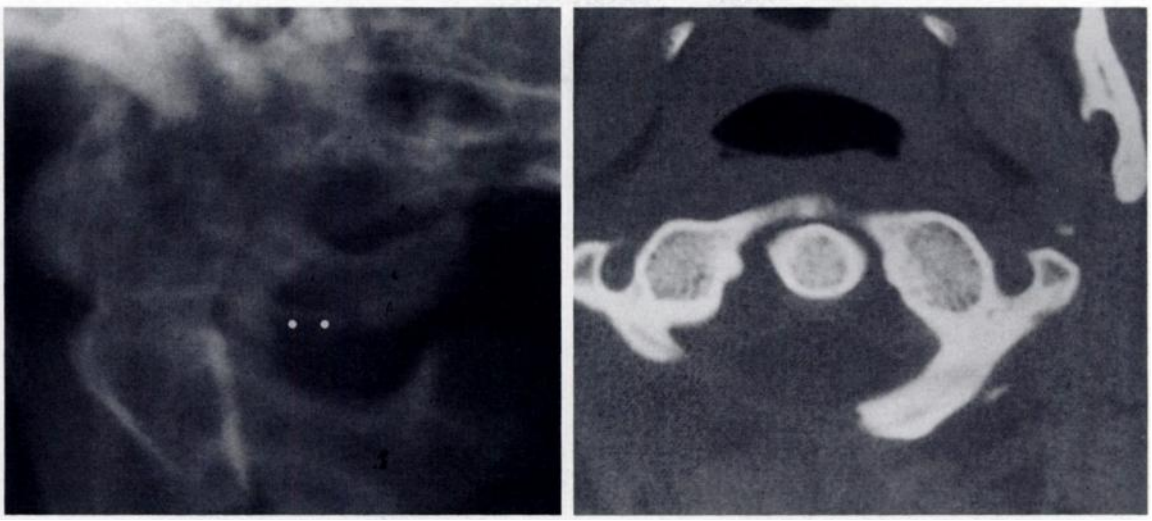

a. b.

**Figure 21.** Posterior arch hemiaplasia. **(a)** Lateral radiograph reveals one posterior arch to be very diminutive (dots), whereas the other is very hyperplastic. The image was obtained to exclude cervical spine trauma, and these findings were initially mistaken for a C-1 arch fracture. Note, however, that both "arches" are intact and completely corticated. **(b)** Axial CT scan helps confirm the hemiaplasia on the right and the hypertrophic appearance of the left posterior arch.

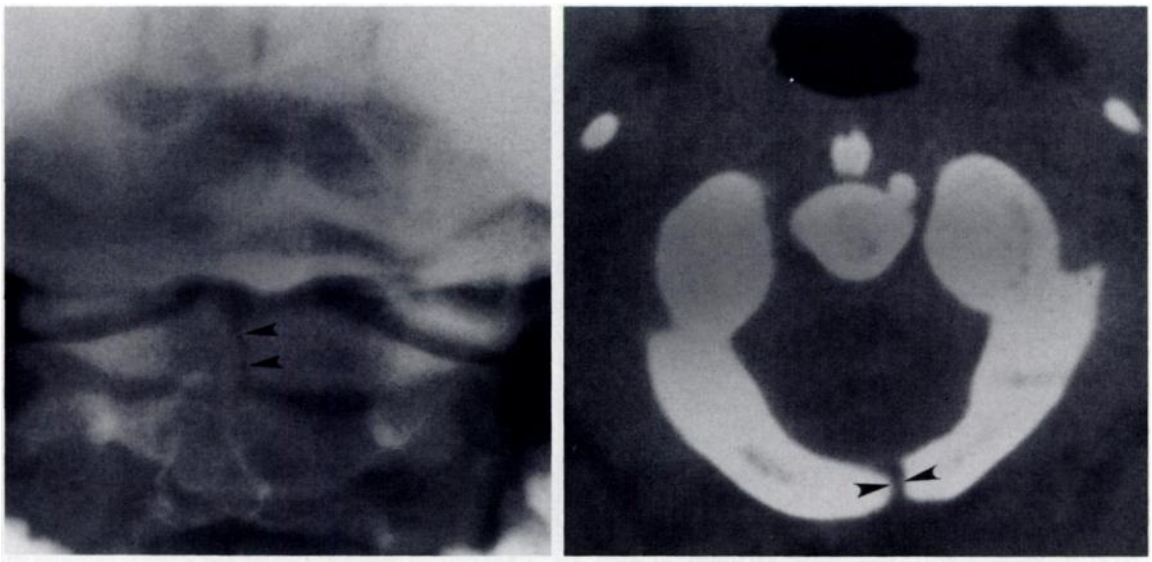

a. b.

**Figure 22.** Posterior arch rachischisis. **(a)** Open-mouth odontoid radiograph demonstrates a pseudofracture overlying the axis (arrowheads). **(b)** Axial CT scan clearly demonstrates the posterior rachischisis (arrowheads).

whereas lateral clefts, through the sulcus of the vertebral artery, account for the remaining 3%. Absence of the arch-canal line, which typically falls on the spinolaminar line, is usually easily identified on lateral plain radiographs in which the two complete posterior arches may be seen in their entirety. Not infrequently, posterior arch rachischisis may be superimposed on the odontoid process or the axis body on the open-mouth odontoid view, simulating a fracture (Fig 22). Obtaining a few axial CT scans can easily solve this dilemma (Fig 22b). Because the posterior arch of the atlas lacks a true spinous process, the often-used term "spina bifida of the atlas" is incorrect, and use of the term "posterior atlas arch rachischisis" is encouraged.

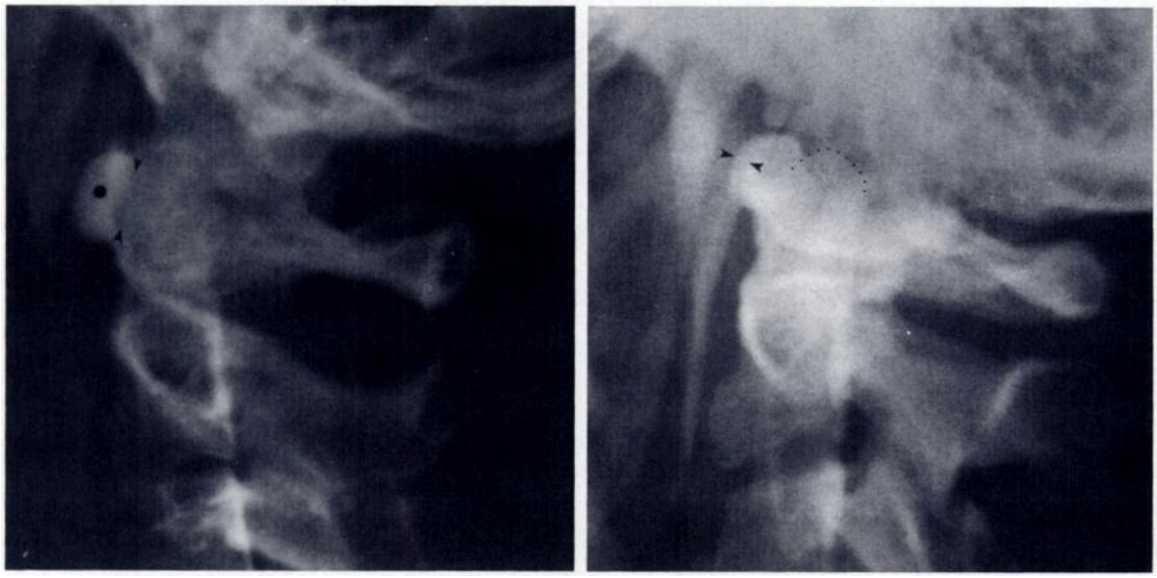

a. b.

**Figure 23.** Anterior atlas arch configurations. **(a)** Normal lateral radiograph reveals a half-moon configuration to the anterior arch (dot) with a 1–2-mm predental space (arrowheads). **(b)** Lateral radiograph of a patient with a split atlas shows an abnormally rounded anterior arch with duplicated anterior margins (arrowheads). The arch seems to overlap the tip of the odontoid process (highlighted by a dotted line) such that a predental space cannot be identified. Note the posterior C-1 arch rachischisis.

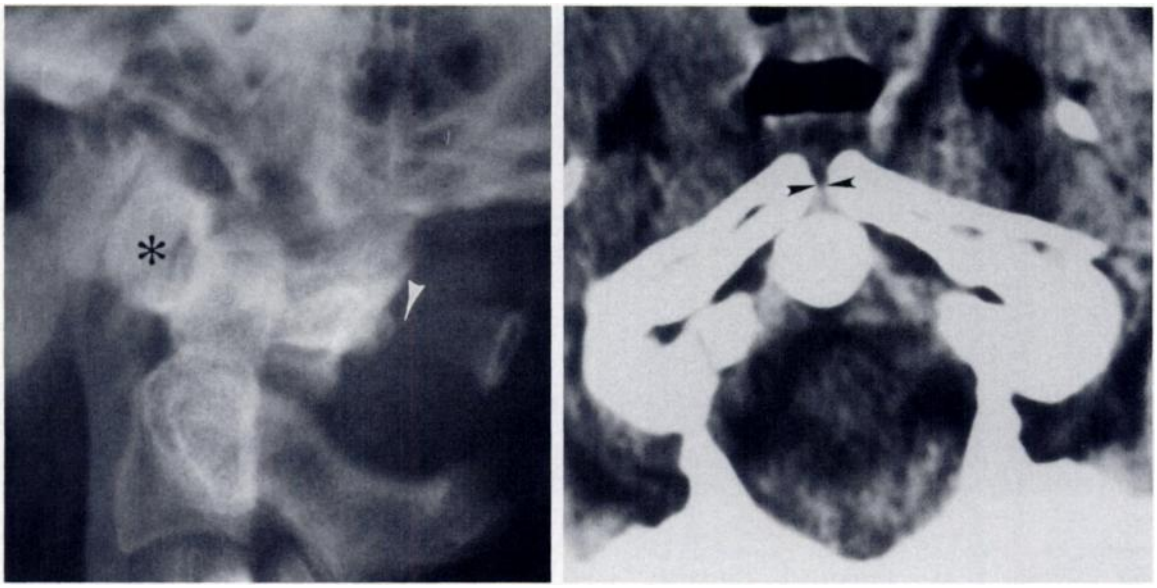

a. b.

**Figure 24.** Split atlas with arch hypoplasia and aplasia. **(a)** Lateral radiograph reveals an enormous anterior C-1 arch (*) that overlaps the odontoid process and a posterior arch defect (arrowhead). **(b)** Axial CT scan demonstrates the anterior rachischisis (arrowheads). The flaring anteriorly produces the "overgrown" appearance seen on the radiograph.

## • Split Atlas

In contrast to posterior arch rachischisis, anterior arch rachischisis is quite rare, occurring in 0.1% of autopsy specimens (1). It is typically encountered in association with posterior rachischisis, in which case the term "split atlas" should be applied (6). Normally, on a lateral radiograph, the anterior arch of the atlas appears crescentic or half-moon-shaped, with dense cortical bone surrounding the medullary cavity and a well-defined predental space

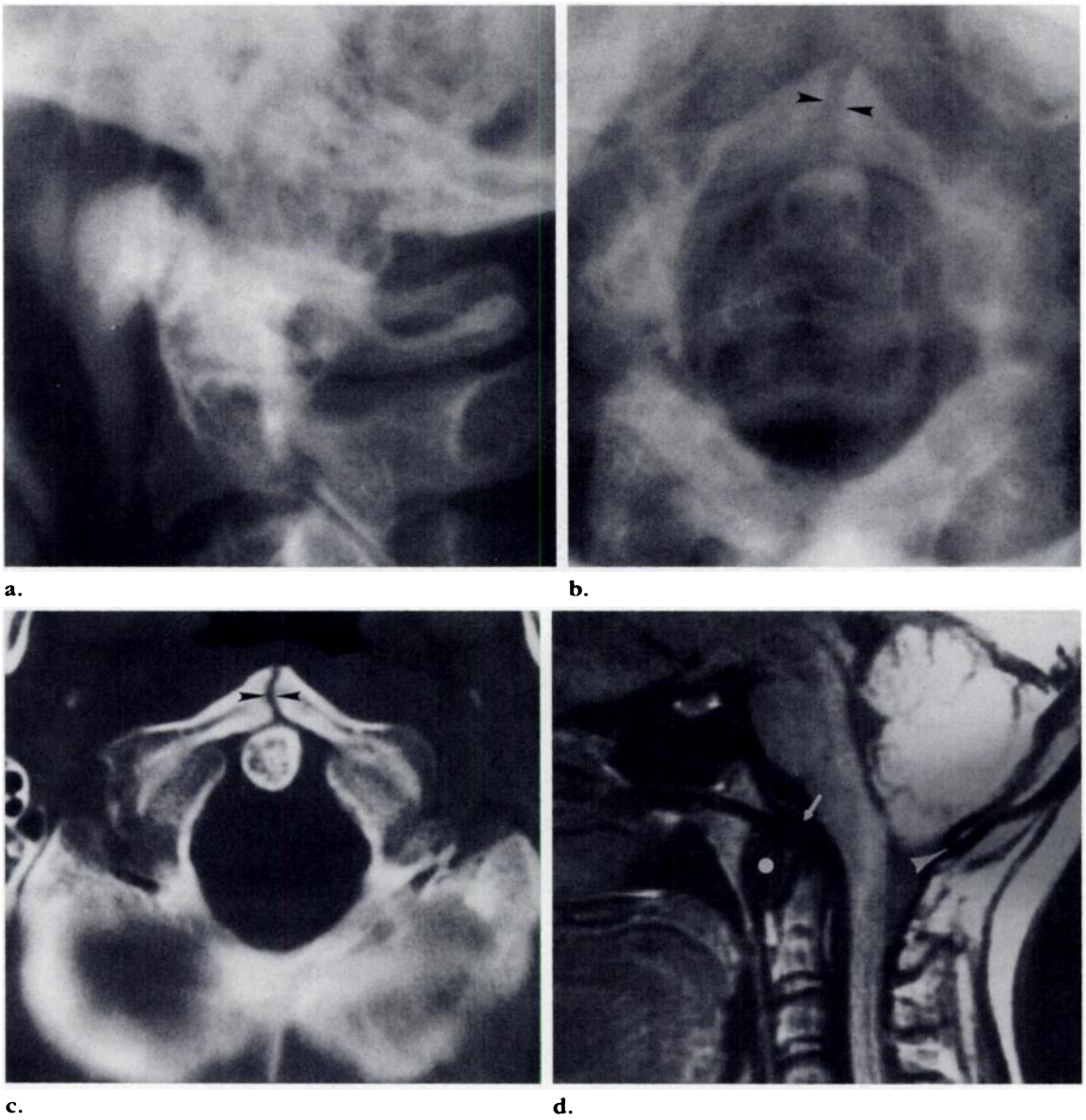


**Figure 25.** Split atlas. **(a)** Lateral radiograph reveals a plump anterior C-1 arch with duplicated margins. A predental space cannot be defined, and posterior rachischisis is evident. **(b)** Submentovertex radiograph demonstrates the wide anterior C-1 rachischisis (arrowheads). **(c)** Axial CT scan helps confirm the wide anterior cleft (arrowheads). **(d)** Midsagittal T1-weighted (600/20) MR image reveals absence of the normal hyperintense marrow of the anterior C-1 arch. Instead, there is a large, rounded cortical signal void (dot) anterior to the odontoid process. No posterior arch cortical margin is identified. The cortical margins of both the basion (arrow) and opisthion (arrowhead) are clearly identified.

(anterior atlantoaxial interval) (Fig 23a). In anterior arch rachischisis, the anterior arch appears fat or plump and rounded in configuration, appearing to "overlap" the odontoid process (making identification of the predental space impossible); the arch may have unsharp, duplicated anterior margins (Fig 23b) (9,13). Associated posterior arch anomalies include hypoplasias and aplasias (Fig 24) and simple posterior arch rachischisis, manifested by absence of the arch-canal line at the C-1 level (Fig 25). Although the anterior rachischisis may occasionally be identified on a submentovertex view of the skull, it is easily appreciated on axial CT scans (Figs 24, 25). To this author's knowledge, the appearance of a split atlas on MR images has not been described. As might be expected, the midsagittal T1-weighted image reveals an absence of the normal marrow signal intensity at the anterior arch level and a large, rounded, cortical signal void where the anterior arch should be (ante-

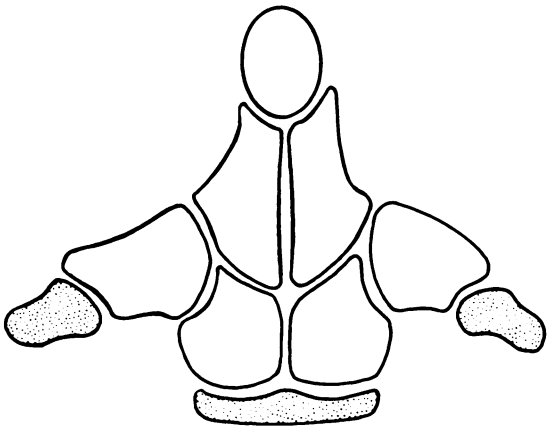

**Figure 26.** Axis ossification centers. Diagram depicts the ossification centers of the axis. Secondary centers are stippled.

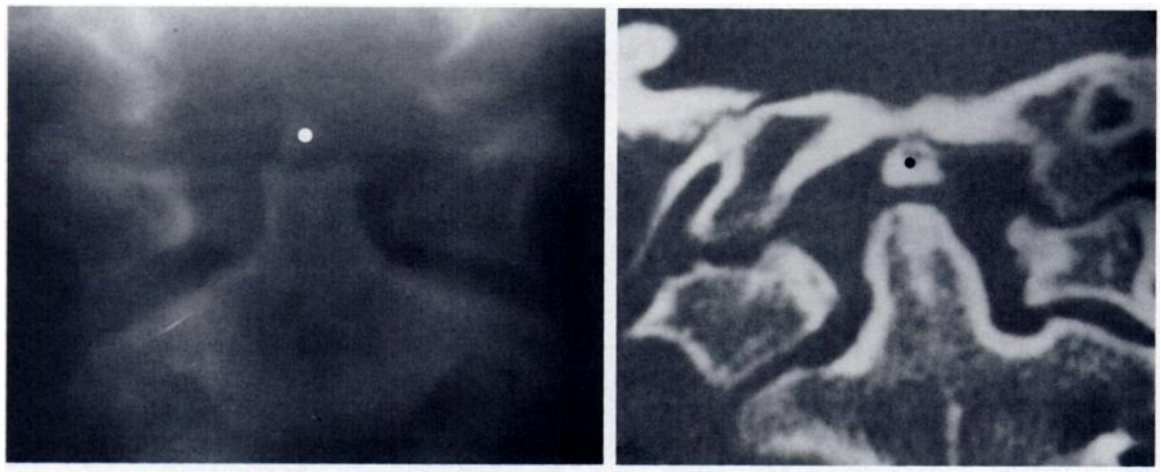

a. b.

**Figure 27.** Persistent ossiculum terminale. Coronal polytomogram **(a)** and coronal CT scan **(b)** reveal lack of fusion of the terminal ossicle of the odontoid process (Bergman ossicle) (dot).

rior arch pseudotumor) (Fig 25d). If the posterior arch rachischisis is midline, no cortical margin of a posterior arch will be identified on the midsagittal MR images either.

Although considered a rare anomaly, multiple reports of the split atlas exist (16–19), and examples of this anomaly are illustrated in a number of textbooks and articles dealing with the CVJ in general (1,2,9,13,20). In most cases referenced, emphasis has been placed on either the posterior arch anomalies or the anterior rachischisis and not the combination of the two anomalies. Although clefts in the arch of the axis are frequently incidental findings, atlas clefts may indicate a dysraphic anomaly of the spinal cord or meninges, and wide clefts with only a fibrous covering may lead to atlas instability (1).

## ■ THE AXIS

With the exception of fusion anomalies, most congenital anomalies of the axis are confined to the odontoid process and are not associated with basilar invagination. As with anomalies of the atlas, these anomalies may simulate traumatic pathologic entities and can best be understood by knowledge of the axis ossification centers (Fig 26).

### • Persistent Ossiculum Terminale

Also called Bergman ossicle, persistent ossiculum terminale results from failure of fusion of the terminal ossicle to the remainder of the odontoid process (Fig 27); the fusion typically is accomplished by 12 years of age (2). On occasion, Bergman ossicle may be confused with a type 1 odontoid fracture (avulsion of the terminal ossicle), and absolute differentiation between the two diagnoses may be difficult (21). Whether traumatic or congenital in

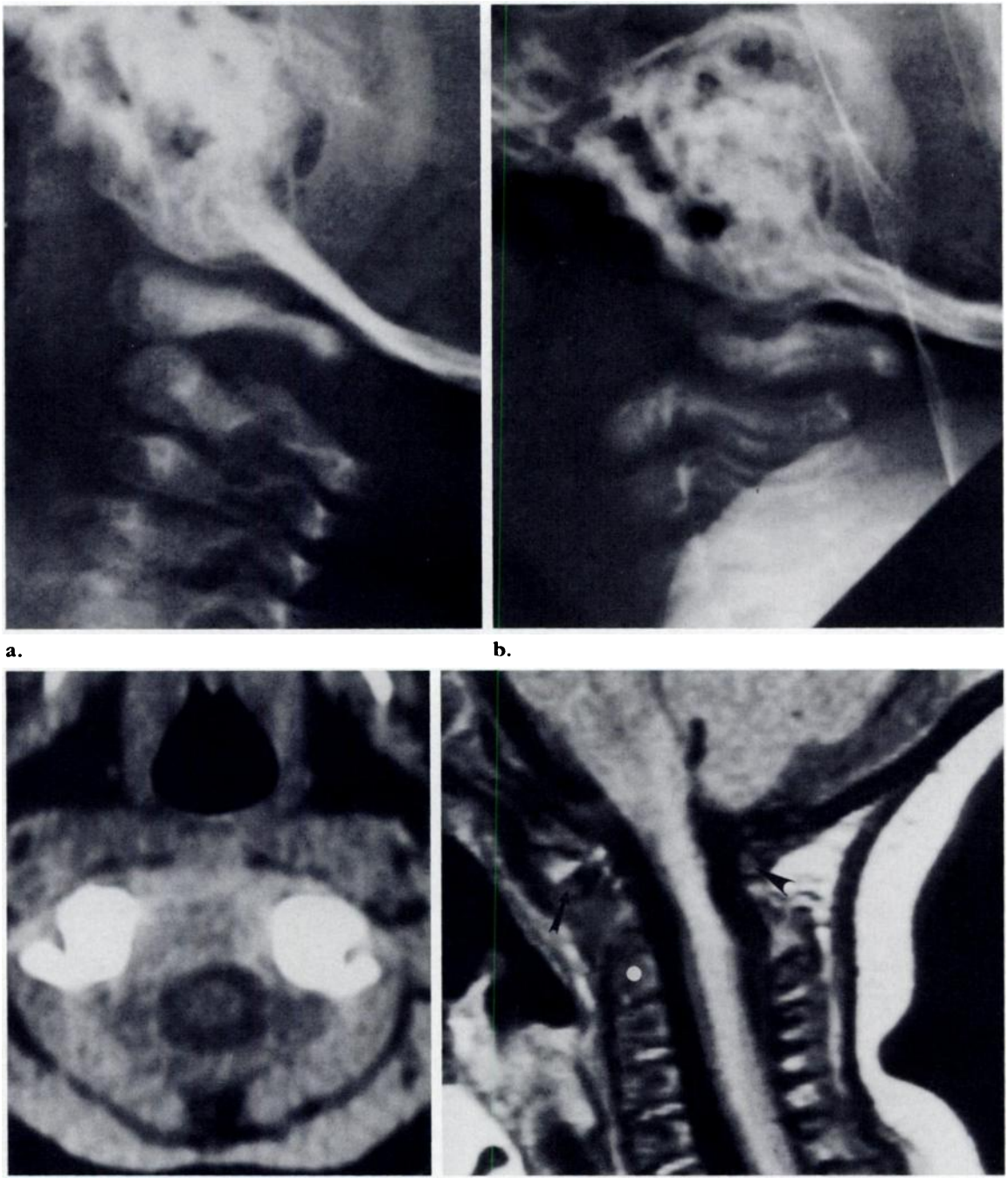

**Figure 28.** Odontoid aplasia. Flexion **(a)** and extension **(b)** radiographs reveal odontoid aplasia with marked subluxation of C-1 and C-2. **(c)** Axial CT scan obtained at the level of the lateral C-1 masses reveals no evidence of an odontoid process. **(d)** Midsagittal T1-weighted (700/20) MR image demonstrates anterior (arrow) and posterior (arrowhead) arches of C-1 and a normal axis body (dot) but no evidence of an odontoid process.

origin, this anomaly is stable when isolated and of relatively little clinical significance. The odontoid process is usually normal in height.

## • Odontoid Aplasia

Total aplasia of the odontoid process is extremely rare (Fig 28) (22). Not infrequently, an os odontoideum may simulate odontoid aplasia, as the os fragment may be perfectly projected over the atlas arch on the open-mouth odontoid view of the upper cervical spine (Fig 29).

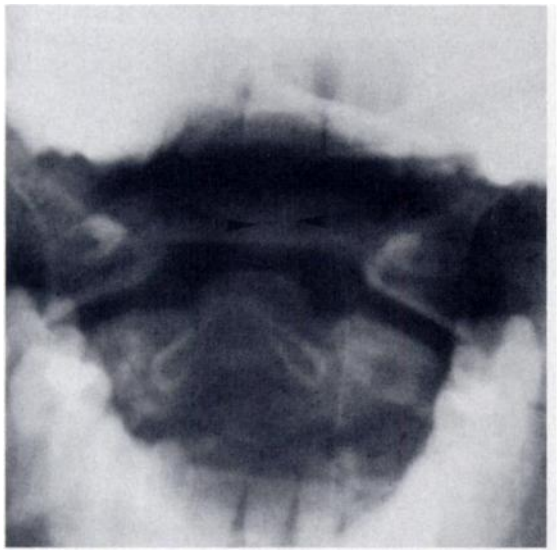

**Figure 29.** Os odontoideum. Findings on this open-mouth odontoid radiograph could be misinterpreted as odontoid aplasia. The os, however, is superimposed on the atlas arch (arrowheads).

## • Os Odontoideum

The term "os odontoideum," first introduced by Giacomini in 1886, refers to an independent osseous structure lying cephalad to the axis body in the location of the odontoid process (Fig 30) (23). The anterior arch of the atlas may appear rounded and hypertrophic, situated too far posterior in relation to the body of the axis (Fig 31) (24). Because the gap between the os odontoideum and the axis body usually extends above the level of the superior articular facet of the axis, cruciate ligament incompetence and atlantoaxial instability are common (25). The degree of instability must be assessed by comparison of flexion and extension studies with plain radiography, polytomography, or MR imaging (Fig 30) (26). When present, instability may lead to substantial narrowing of the spinal canal and cord compression at the level of C-1. Occasionally, differentiation between an os odontoideum and a type 2 odontoid fracture on a lateral radiograph may be problematic. In the presence of an os odontoideum, the axis body has a well-corticated convex upper margin, and the anterior atlas arch ap-

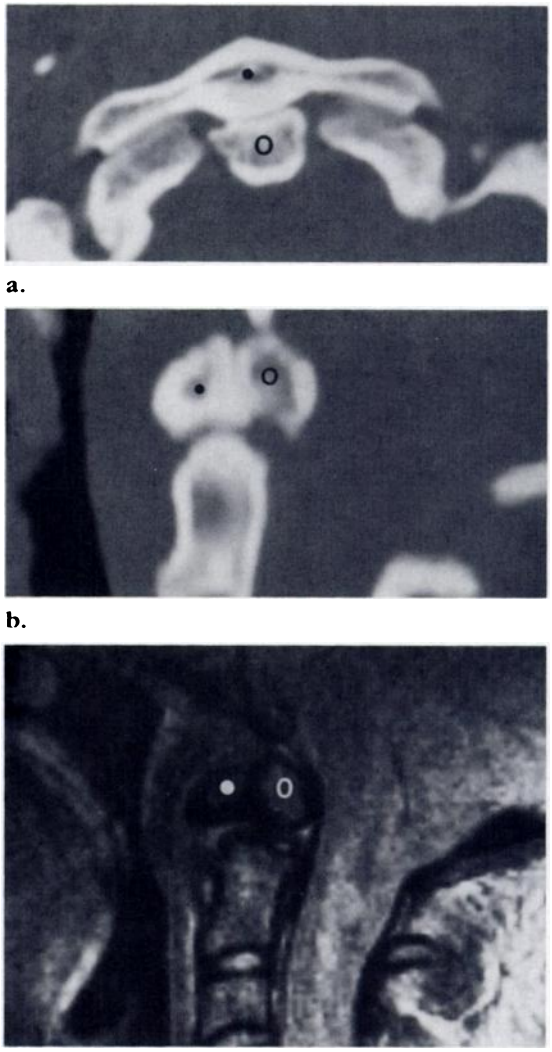


**Figure 31.** Os odontoideum. Axial **(a)** and midsagittal **(b)** reconstructed CT images reveal marked hypertrophy of the anterior C-1 arch (dot). The margins of the axis body, the os (*O*), and anterior arch are all well corticated. **(c)** Midsagittal proton density (3,000/45) MR image reveals thick cortical signal void of the anterior C-1 arch (dot), the os fragment (*O*), and the axis body.

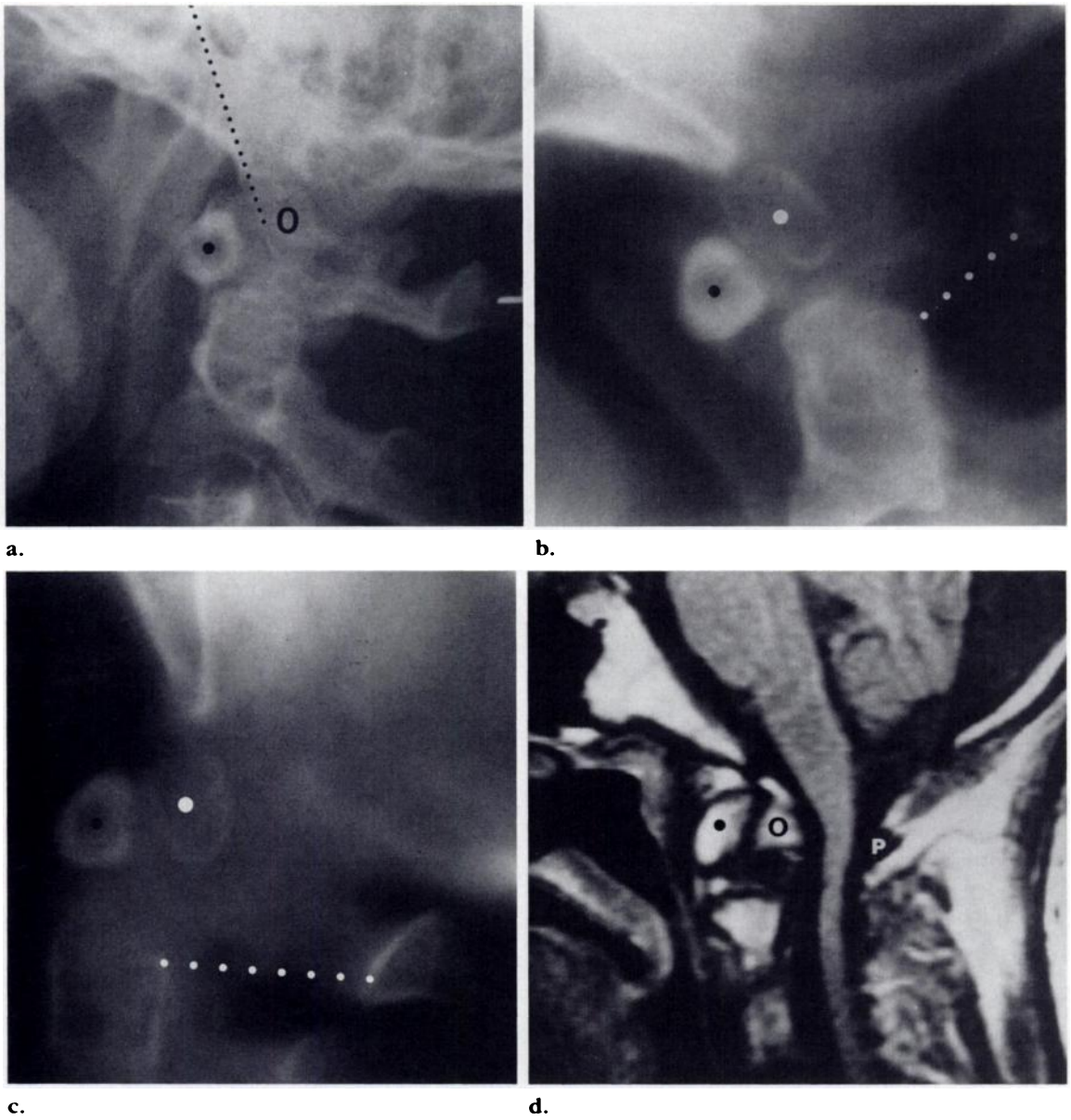


**Figure 30.** Os odontoideum. **(a)** Lateral plain radiograph reveals absence of the odontoid process, with the suggestion of an os odontoideum (*O*). The rounded anterior atlas arch (dot), which partially lies above the axis body, adds further support to this diagnosis; the Wackenheim clivus baseline (dotted line) falls tangent to the anterior aspect of the os. **(b, c)** Flexion **(b)** and extension **(c)** midline polytomograms reveal marked instability as the os (white dot) and atlas (black dot) move in relation to the axis body. Note the narrowing of the spinal canal resulting from the subluxation in flexion compared with that in extension (dotted line). **(d)** Midsagittal T1-weighted (600/20) MR image easily demonstrates the hypertrophic anterior arch of C-1 (dot), the os (*O*), and the posterior arch of C-1 (*P*).

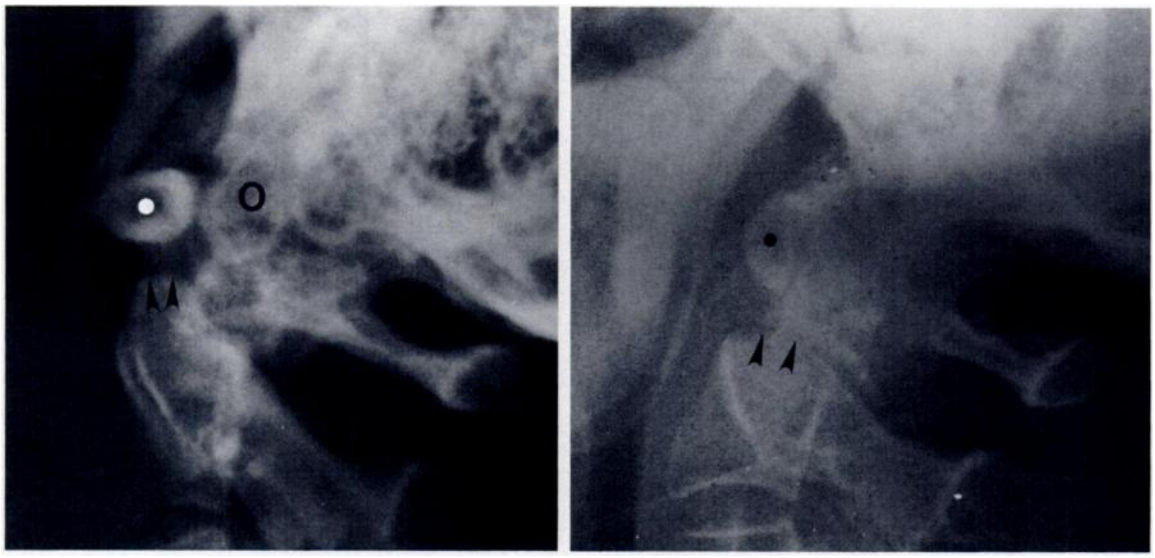


a. b.

**Figure 32.** Os odontoideum or fracture? **(a)** Lateral radiograph of a patient with os odontoideum (*O*) reveals a well-corticated convex upper margin to the body of the axis (arrowheads) and a rounded hypertrophic configuration to the anterior atlas arch (dot). **(b)** Lateral radiograph of a patient with a type 2 odontoid fracture reveals a normal half-moon appearance to the anterior atlas arch (dot) and a flattened, straight configuration to the upper margin of the axis (arrowheads). The odontoid and atlas are posteriorly displaced.

pears hypertrophic and rounded, rather than half-moon-shaped (Fig 32). In contrast, the type 2 odontoid fracture is typically associated with a flattened, sharp, uncorticated margin to the upper axis body and a normal, half-moon-shaped appearance to the anterior atlas arch (Fig 32).

## ■ SUMMARY

Understanding and evaluation of CVJ relationships can be simplified by identification of relatively few anatomic landmarks, basic knowledge of the development of structures constituting the CVJ (occiput, atlas, and axis), and application of some simple craniometric measurements. This article has focused on anomalies of the occiput producing basilar invagination and developmental abnormalities of the atlas and axis that, although typically not associated with basilar invagination, may be confused with traumatic pathologic entities. Armed with this knowledge, accurate assessment of the CVJ is possible, with the liberal use of multiple imaging modalities and orthogonal planes. With the widespread availability of MR imaging, which is especially well suited for evaluation of the CVJ by virtue of direct sagittal imaging capabilities, renewed understanding and review of CVJ anatomy and congenital anomalies become important for all radiologists.

**Diagnoses for cases in Figure 1:** Fig 1a, basiocciput hypoplasia with basilar invagination (see Fig 15 for more explanation); Fig 1b, os odontoideum (see Fig 30); Fig 1c, atlantooccipital assimilation with anterior atlantoaxial subluxation (see Fig 19b); Fig 1d, condylus tertius and platybasia (see Fig 10); and Fig 1e, split atlas (see Fig 25d).

**Acknowledgments:** Special thanks to J. Carlos Chazo, D. Laurie Persson, BA, BSAAM, and David M. Abell, BS, for their excellent medical illustration and photographic assistance and to Shelia A. Wright for her editorial assistance.

## ■ REFERENCES


1. vonTorklus D, Gehle W. The upper cervical spine. New York, NY: Grune & Stratton, 1972.
2. VanGilder JC, Menezes AH, Dolan KD. The craniovertebral junction and its abnormalities. New York, NY: Futura, 1987.
3. Chamberlain WE. Basilar impression (platybasia). Yale J Biol Med 1939; 11:487–496.
4. McGregor J. The significance of certain measurements of the skull in the diagnosis of basilar impression. Br J Radiol 1948; 21:171–181.
5. Menezes AH, VanGilder JC. Anomalies of the craniovertebral junction. In: Youman JR, ed. Neurological surgery. 3rd ed. Philadelphia, Pa: Saunders, 1990; 1359–1420.
6. Wackenheim A. Roentgen diagnosis of the craniovertebral region. New York, NY: Springer Verlag, 1974.
7. Dolan KD. Cervicobasilar relationships. Radiol Clin North Am 1977; 15:155–166.
8. El Khoury GY, Wener MH, Menezes AH, et al. Cranial settling in rheumatoid arthritis. Radiology 1980; 137:637–642.
9. Wackenheim A. Cervico-occipital joint. Berlin, Germany: Springer, 1985.
10. Bernini FP, Elefante R, Smaltino F, et al. Angiographic study on the vertebral artery in cases of deformities of the occipitocervical joint. AJR 1969; 107:526–529.
11. McRae DL, Barnum AS. Occipitalization of the atlas. AJR 1953; 70:23–46.
12. Vakili ST, Aguilar JC, Muller J. Sudden unexpected death associated with atlanto-occipital fusion. Am J Forensic Med Pathol 1985; 6:39–43.
13. Gehweiler JA, Daffner RH, Robert SL. Malformations of the atlas vertebra simulating the Jefferson fracture. AJNR 1983; 4:187–190.
14. Schulze PJ, Buurman R. Absence of the posterior arch of the atlas. AJR 1980; 134:178–180.
15. Dalinka MK, Rosenbaum AE, Van Houten F. Congenital absence of the posterior arch of the atlas. Radiology 1972; 103:581–583.
16. Kuhne D. Fissures in the anterior arch of the atlas diagnosed by careful study of the lateral radiographs. Neuroradiology 1977; 4:205–208.
17. Geens JG, Schuur KH. A rare developmental variant of the axis. Eur J Radiol 1985; 5:12–13.
18. Chambers AA, Gaskill MF. Midline anterior atlas clefts: CT findings. J Comput Assist Tomogr 1972; 16:868–870.
19. Dorne HL, Just N, Lander PH. CT recognition of anomalies of the posterior arch of the atlas vertebra: differentiation from fracture. AJNR 1986; 7:176–177.
20. Cone RO, Flourney J, MacPherson RI. The craniocervical junction. RadioGraphics 1986; 1:1–37.
21. Anderson LD, D'Alonzo RT. Fractures of the odontoid process of the axis. J Bone Joint Surg [Am] 1974; 56:1663–1674.
22. Gillman EL. Congenital absence of the odontoid process of the axis: report of a case. J Bone Joint Surg [Am] 1959; 41:345–348.
23. Giacomini C. Sull' esistenaza dell' "os odontoideum" nell' uomo. Gior Acad Med Torino 1886; 49:24–28.
24. Holt RG, Helms CA, Munk PL, Gillespy T. Hypertrophy of C-1 anterior arch: useful sign to distinguish os odontoideum from acute dens fracture. Radiology 1989; 173:207–209.
25. Menezes AH, VanGilder JC, Graf CJ, McDonnell DE. Craniocervical abnormalities: a comprehensive surgical approach. J Neurosurg 1980; 53:444–455.
26. Thomason M, Young JWR. Os odontoideum. Skeletal Radiol 1984; 11:144–146.